In Vivo Toxicity of Upconversion Nanoparticles. Overview. Part I

Irina Yu. Yanina* **and Vyacheslav I. Kochubey**
Institute of Physics, Saratov State University, 83 Astrakhanskaya str., Saratov 410012, Russian Federation
*e-mail: irina-yanina@list.ru

Abstract. This review synthesizes current research on the *in vivo* dark toxicity of upconversion nanoparticles (UCNPs) for biomedical applications, including luminescent imaging, diagnostics, and photoinduced therapy. The aim is to assess key toxicity determinants – nanoparticle type, surface coating, concentration, and dose relative to body weight – and to establish safe exposure thresholds. Analysis of comprehensive histological and biochemical studies indicates that UCNPs generally exhibit low toxicity under tested conditions. The most non-toxic concentration identified across studies is 2 mg/mL. For mice, the maximum permissible dose for short-term exposure (12 h) is 10 mg/kg, and for long-term exposure (120 days) is 50 mg/kg. For rats, a dose of 5 mg/kg is safe for both short- and long-term studies. While positively charged coatings (e.g., PEI) enhance cellular uptake, they may increase cytotoxicity compared to neutral or negatively charged coatings (e.g., PAA, PEG). Dissolution of UCNPs releasing rare-earth and fluoride ions contributes to dark toxicity, but biocompatible shells (silica, PEG) reduce this effect. Overall, UCNPs demonstrate favorable biocompatibility at established doses, supporting their continued development for *in vivo* theranostic applications. This review is the first of three parts; subsequent parts address phototoxicity and toxicity of multimodal particles.

Keywords: toxicity; upconversion nanoparticles; concentration; dose.

Paper #9595 received 17 Apr 2026; revised manuscript received 21 May 2026; accepted for publication 26 May 2026; published online 7 Sep 2026. doi: 10.18287/JBPE26.12.030201.

1 Introduction

The field of *in vivo* cellular and molecular research has experienced significant methodological advancements in imaging over recent decades [1–5]. Among the most promising techniques is luminescent imaging, which offers a noninvasive means to elucidate tissue architecture, detect specific biomolecules, and monitor biological processes in real time [6–10].

The foundation of this approach lies in the use of highly luminescent agents. For these probes to be effective in biomedical applications, they must satisfy several key requirements. First, they should be amenable to chemical modification, allowing researchers to enhance their biocompatibility or confer targeting capabilities [11–13]. Second, they must exhibit low toxicity to ensure minimal adverse effects on living systems. Third, and critically, they should absorb and emit light within the 650–1450 nm range – encompassing the red and near-infrared (NIR) regions of the spectrum.

This spectral window confers significant advantages for *in vivo* imaging. Notably, light in this range experiences minimal absorption by biological tissues (with the exception of water absorption bands), enabling excitation photons to penetrate deeply into living tissue [14]. This property stands in stark contrast to visible light, which is substantially attenuated by tissue components.

Another pivotal advantage of NIR visualization lies in its ability to improve the signal-to-noise ratio. Since endogenous autofluorescence predominantly occurs in the visible spectrum (400–650 nm), imaging in the NIR range drastically reduces background interference [15]. This spectral separation enhances detection sensitivity,

making it possible to reliably identify targets even at low concentrations.

Furthermore, NIR photons exhibit reduced scattering in biological tissues compared to visible light. This characteristic translates into superior spatial resolution and sharper image contrast, particularly beneficial when imaging dense or heterogeneous tissues. The combination of deep tissue penetration, low background noise, and high resolution positions NIR-emitting luminescent probes as invaluable tools for *in vivo* applications [16].

Ongoing research continues to focus on optimizing probe design – particularly through surface functionalization and fine tuning of emission properties – to further expand the utility of luminescent imaging in preclinical and potentially clinical settings.

Moreover, the luminescence properties of phosphors are sensitive to their environment, which enables their use as biosensors for detecting various biological parameters. These include: intracellular temperature (via luminescent thermometers); oxygen levels (for monitoring oxygen content in living systems); specific molecules (such as proteins, amino acids, antibiotics, and DNA) and various ions [17–24].

A special class of phosphors can transfer absorbed excitation energy to molecular triplet oxygen ($^3O_2$), promoting it to the excited singlet state ($^1O_2$) [25, 26]. Singlet oxygen is highly chemically reactive: when produced within cells, it can damage cellular structures and trigger cell death [27]. This mechanism underpins photodynamic therapy – one of the most promising approaches to cancer treatment [26].

Consequently, luminescent compounds have found wide-ranging applications in biology and medicine. This has spurred a significant increase in research publications focused on developing luminescent materials for biological imaging, disease diagnostics, and therapeutic applications in recent years.

Among luminescent materials, upconversion nanoparticles (UCNPs) stand out as particularly promising. Their emission arises from cooperative energy transfer processes. The key feature of UCNPs is that excitation requires the absorption of at least two photons, which enables excitation in the infrared (IR) region [15]. Meanwhile, the resulting luminescence exhibits shorter wavelengths — a phenomenon driven by the anti-Stokes process.

This unique mechanism provides UCNPs with an important additional advantage. Since biological tissues typically exhibit luminescence at longer wavelengths compared to the excitation wavelength, the background luminescence of biotissues at the UCNP emission wavelengths is substantially reduced [15]. Consequently, UCNPs not only retain the beneficial properties common to luminescent materials but also enable significantly improved signal-to-background ratios in biological imaging applications.

The use of nanoparticles in medicine and biology necessitates careful consideration of their potential toxicity. Due to their small size, nanoparticles inherently pose toxicity risks – their high surface-area-to-volume ratio enhances reactivity and may lead to unintended biological interactions [28–30]. The influence of various factors on *in vivo* dark toxicity is shown in Fig. 1.

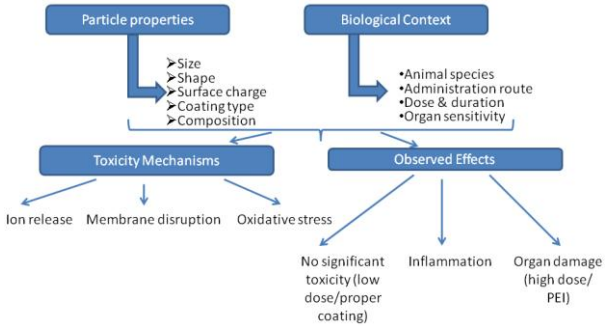

Fig. 1 Hierarchical diagram of factors affecting *in vivo* dark toxicity of UCNPs.

However, it is crucial to emphasize that the toxicity of UCNPs is not uniform; it depends on a range of physicochemical and physiological factors.

Physicochemical properties that influence toxicity include: particle size, shape, surface area, chemical composition and surface charge and functionalization (e.g., coating with biocompatible polymers) [28–30].

Physiological factors that modulate toxicity comprise: the specific disease context (e.g., inflamed vs. healthy tissue), individual genetic variations, metabolic state of the organism, route of administration and dose and duration of exposure [31].

Thus, assessing UCNP safety requires a comprehensive evaluation that integrates both material characteristics and biological context. This enables the design of safer nanomaterials and informed risk-benefit analyses for biomedical applications [32].

The recommended size for optimal penetration of NPs is below 100 nm. However, this size may also pose a risk of toxicity due to their potential to penetrate cellular structures and organs via the circulatory system.

One crucial aspect of using UCNPs in biomedical applications lies in ensuring their biocompatibility on cells and or organisms [32]. To achieve this several chemical groups, including silica [33–35], polyethyleneimine (PEI) [36–39], polyvinyl pyrrolidone (PVP) [39], polyacrylic acid (PAA) [39–41], and polyethylene glycol (PEG) [42], have been used for this purpose. Additionally, UCNPs must be functionalized with different ligands that specifically target the desired cells and organs.

The increased surface area leads to higher solubility, causing compounds that would normally be insoluble to dissolve. As a result, toxicity can occur when these dissolved products – consisting of molecules and ions from the nanoparticle – enter living cells.

Increasing the relative surface area of nanoparticles not only affects their solubility, but also enhances their chemical activity. This can lead to increased toxicity, as the nanoparticles' chemical activity can cause harmful

effects. The toxicity of nanoparticles depends on their composition, the materials used to create their shells, and the surface charge of the nanoparticles [28–30].

When analyzing the causes of toxicity, it is also important to consider the surface charge of nanoparticles. This charge depends on the presence or absence of a shell around the nanoparticle. So-called "bare" nanoparticles, which are nanoparticles without a protective shell, can be obtained by either removing of the shell by reacting with acids (HCl) or by replacing it with other ligands (BF^{4-}). However, it should be noted that the term "bare" is somewhat arbitrary, as these nanoparticles quickly acquire a negative charge when exposed to aqueous solutions due to the presence of OH- ions.

It is important to note that the toxicity of nanoparticles is essential for their therapeutic use. This toxicity may lead to apoptosis or necrosis of the cells that are penetrated by the nanoparticles. The aim of targeted therapy is to specifically deliver nanoparticles to pathological cells, so that these cells experience the toxic effects of treatment.

However, it is also important to consider the potential undesirable toxic effects that can arise.

Toxicity can occur at different levels, including the cellular, subcellular, and molecular levels, as well as in altered organ function.

Nanoparticles injected into the bloodstream can reach the liver, spleen, lungs, heart, and brain [36]. The biologically inert shells of these nanoparticles allow them to circulate in the blood for a long time, leading to their accumulation in various organs. The presence of addressable molecules on the nanoparticles' shells can reduce their circulation time.

The toxicity of nanoparticles plays a crucial role in their application in photodynamic therapy and other biological uses and serves as a primary selection criterion. Depending on the intended application, particles with different types of coatings or composition are developed. There are several reviews on the toxicity of UCNPs [43–45]. However, the data presented in the literature are often contradictory, particularly regarding the maximum permissible concentration of nanoparticles. And despite the large number of studies on toxicity and antitumour effects in animals, the authors sometimes fail to provide important information such as the dose and concentration of particles used. On the other hand, as a rule, the authors do not investigate the mechanism of toxicity. The authors investigate the toxicity of a certain type of nanoparticles with a given coating for various cells, organisms and organs.

2 *In Vivo* Dark Toxicity of Nanoparticles

Nanoparticle toxicity can be divided into two main types: intrinsic toxicity and light-activated toxicity (phototoxicity).

Phototoxicity is usually caused by the generation of reactive oxygen species (ROS) or nitrogen. Both the nanoparticle surface itself and its shell can participate in the generation process. To increase activity, the shell may include photodynamic dyes. In this case, photoexcitation of the dye occurs via photons of nanoparticle luminescence, which is excited by external radiation. The resulting products can cause DNA damage, which not only affects cell growth through protein oxidation but also impacts mitochondrial respiration [32].

As mentioned earlier, one of the causes of dark toxicity is the dissolution of nanoparticles. This process leads to the formation of ions of rare earth elements and fluorine, which can have a negative impact on cells and the body.

The dissolution of nanoparticles in the blood may generate yttrium ions, which could affect bone and bone marrow cell function [46]. Additionally, there is a report of the possibility of toxicity from the substitution of calcium ions (Ca^{2+}) with gallium ions (Ga^{3+}) [47].

The effect of lanthanides on blood composition is also well-known [45].

In the absence of lanthanide ions in UCNPs, their toxicity is reduced. Tian et al. intravenously administered 1200 mg/kg of upconversion nanocapsules to mice over 60 days [48]. Under these conditions, no significant toxicity was observed, as evidenced by body weight determination, histological and hematological analyses, and biochemical blood tests. Meanwhile, Yang et al. demonstrated that at a dose of 28 mg/kg, UCNPs caused temporary lung and liver damage in mice [49].

BALB/c mice were injected with 200 μL of high-dose solution (2.0 mg [Y]/kg mouse weight) and low-dose solution (0.2 mg [Y]/kg mouse weight) PEG-coated $NaYF_4$:Yb^{3+}/Er^{3+} nanoparticles through the tail vein for the experimental group, while the control group received an equivalent amount of phosphate-buffered saline (PBS). Major organs were collected 24 and 72 h later, sectioned and subjected to haematoxylin & eosin (H&E) staining to observe histopathological changes for toxicity assessment [50]. There was no notable histopathological damage in the major organs of the control mice. The heart, liver, spleen, lungs, and kidneys of the experimental group exhibited general consistency with those of the control mice, show casing normal tissue cell morphology and an absence of acute inflammatory responses. Moreover, no inflammatory reactions were detected in tissue sections taken at 24 h and 72 h post-injection, suggesting that neither short-term nor prolonged exposure to UCNPs induced organ damage in the mice. The metabolic and clearance pathways of UCNPs in mice were investigated by quantifying yttrium levels in feces and urine. The study revealed that UCNPs were primarily metabolized through fecal excretion within the initial four hours, shifting towards urinary excretion thereafter. Complete elimination was achieved within 72 h.

The dissolution rate of nanoparticles depends on the condition of their surface. If a nanoparticle's surface is not stabilized, it is likely to dissolve more easily than if it is protected by specialized coatings. It is important to consider the potential toxicity of these coatings,

however, as they may also affect the dissolution process.

Shells made of silica, zinc sulfide, or polymers are often used to enhance the biocompatibility of nanoparticles and decrease their solubility. However, research has shown that silica can interact with cells and cause inflammation, which may be linked to various diseases, such as rheumatoid arthritis, sclerosis, lupus, and chronic kidney disease [51, 52]. At the same time, the silica coating reduces the solubility of nanoparticles and the cytotoxicity caused by fluoride ion release during dissolution [53].

Studies on the biocompatibility of nanoparticles coated with a SiO_2 layer have shown that they exhibit low dark cytotoxicity, can penetrate cells, and remain inside for a considerable time. For instance, intravenous administration of coated with SiO_2 $NaYF_4$:25%Yb^{3+}, 0.3%Tm^{3+} particles at a dose of 10 mg/kg to laboratory rats resulted in no adverse health effects or behavioral changes throughout the study (7 days) [33, 34]. Recently, it was shown that oral or intravenous administration of $NaYF_4$:Yb/Er@SiO_2 nanoparticles does not exhibit significant toxicity in mice, even at high doses of 100 mg/kg body weight [35]. The study revealed that the nanoparticles mainly accumulate in bones, the stomach, and intestines upon oral administration, whereas intravenous injection leads to accumulation primarily in the liver and spleen.

The Zhang group reported that $NaYF_4$ nanoparticles coated with SiO_2 are predominantly excreted from the bodies of mice by the 7th day after injection at a dose of 10 mg/kg [33]. A review of the properties and toxicity of functionalized UCNPs is provided in studies [54–56].

The experimental results show that the positively charged UCNP@SiO_2-PEG-NH_2 has a stronger cytotoxic effect and better cell internalization ability than the negatively charged UCNP@SiO_2-COOH and UCNP@SiO_2-PEG. This charge-based difference in cytotoxicity may be caused by the redox stress caused by UCNP@SiO_2, as well as the release of metal ions and ligands [57].

The toxicity of nanoparticles varies depending on the object they affect. In a study of the toxicity of UPNPs on keratinocytes, the toxicity was maximal when coated with PEI, weak cytotoxicity when coated with polymaleic acid (PMAO), and virtually non-toxic in the case of low molecular weight tetraethylammonium hydroxide (TMAH) [58]. When exposed to nerve cells, the toxicity differs. The TMAH coating allows nanoparticles to be hydrophilized by replacing oleic acid on their surface with a polymer, resulting in the appearance of hydroxide (OH-) radicals on the surface. This causes the nanoparticles to become negatively charged, similar to when coated with PMAO. However, the surface potential of PMAO is twice that of TMAH in this case.

There is no clear consensus on the toxicity of nanoparticles coated with PEI. PEI and nanoparticles based on it may cause toxic effects in cells, and the toxicity increases with molecular weight and branching degree. These toxic effects are associated with the interaction between the cationic polymer and cell membranes, which can disrupt them. PEI can destroy cellular and mitochondrial membranes, leading to necrosis or apoptosis.

However, there are also studies showing that introducing PEI into nanoparticle's shells does not significantly affect their toxicity [59].

When PEI was used as a coating for UCNPs ($NaYF_4$:Yb^{3+},Er^{3+}) and administered intravenously to laboratory rats at concentrations of 1.5, 10, 15, and 25 μg/mL and doses of 10 mg/kg, no toxic effects on cells or mice were observed [36]. Studies examined PEI-modified $NaYF_4$:Yb,Er nanoparticles with different administration methods in mice: intravenous, intraperitoneal, and intragastric (at doses of 10 mg/kg) [37, 38]. Following intraperitoneal administration, PEI@UCNPs accumulated significantly in the spleen for 30 days. In contrast, intragastric administration resulted in a decrease in accumulation over time in various body tissues, with particles primarily detected in the ileum and cecum, while their presence in other organs was relatively low. For intravenous administration, UCNPs demonstrated excretion from the body within 30 days and a gradual decrease in accumulation in the spleen.

Thus, high molecular weight PEI and high concentrations can be cytotoxic [60]. For medical purposes, modified forms of PEI are being developed, such as pegylation and acetylation, to reduce surface charge and toxicity.

For example, in a study, the effect of PEI, PVP, and PAA coatings on the cytotoxicity and cellular penetration of $NaYF_4$:Yb/Er nanoparticles was investigated [39]. These polymers carry different charges: PVP is neutral, PEI is positively charged, and PAA is negatively charged. Thus, this study aimed to explore the impact of surface charge on particle biocompatibility. $NaYF_4$:Yb/Er-PVP was synthesized via solvothermal methods, while $NaYF_4$:Yb/Er-PEI and $NaYF_4$:Yb/Er-PAA were obtained by replacing PVP through interactions with PEI and PAA in heated solution. Cytotoxicity tests on HeLa and U87MG (human glioblastoma) cell lines revealed that the least toxic material was the negatively charged $NaYF_4$:Yb/Er-PAA. At the same time, confocal microspectroscopy using 980 nm laser excitation on the same cell lines showed that $NaYF_4$:Yb/Er-PEI exhibited significantly higher penetration efficiency: $NaYF_4$:Yb/Er-PEI > $NaYF_4$:Yb/Er-PVP > $NaYF_4$:Yb/Er-PAA. This can be explained by the negative charge of the cell membrane, which has a greater affinity for positively charged $NaYF_4$:Yb/Er-PEI particles. For $NaYF_4$:Yb/Er-PEI, which demonstrated the highest penetration ability, the mechanism of cellular entry was studied, showing that the particles enter cells via clathrin-mediated endocytosis.

PAA is a non-toxic and biocompatible substance that can be biodegraded. However, there is still some uncertainty about the potential toxicity of PAA-coated

nanoparticles, as there is no clear consensus on this issue. Additionally, there is currently no direct evidence to support the toxicity of these nanoparticles themselves.

Intravenous administration of functionalized $NaYF_4$:20%Yb^{3+}, 1%Tm^{3+}-PAA particles at a dose of 15 mg/kg to mice did not result in toxic effects on cells or mice, with only minor hyperplasia observed in the per arteriolar lymphoid sheath of the white pulp [40]. Additionally, no significant toxicity was observed over a 115-day period [41].

In contrast, PEG-coated nanoparticles have been shown to be non-toxic due to the use of PEG to modify their surface. This modification process can improve the biophysical and chemical properties of the nanoparticles, such as reducing the adsorption of plasma proteins onto their surface and increasing their circulation time within the body.

In study, mice were intravenously injected with 200 μL of UCNPs ($NaYF_4$:Yb^{3+}/Tm^{3+} coated with PEG or functionalized with PAA) at a concentration of 2 mg/mL (dose of 20 mg/kg), and their condition was analyzed at various time points post-injection (3, 7, 20, 40, and 90 days, with five mice per time point) [42]. No noticeable toxic side effects were observed in laboratory animals.

UCNPs β-$NaYF_4$:20%Yb^{3+}, 2%Tm^{3+}, coated with octylamine-PAA or 1,2-distearoyl-sn-glycero-3-phosphoethanolamine-PEG, when intravenously injected into the vena cava at a volume of 200 μL and concentration of 2 mg/mL (dose of 20 mg/kg), did not cause any evident histological damage or organ impairment. Biochemical, hematological, and histological analyses remained normal at a dose of 20 mg/kg. UCNPs can be partially degraded or processed within macrophage cells without significant release [42].

In paper, spherical or hexagonal NaYF:Yb,Er UCNPs with sizes of 25 nm (S-UCNPs) and 120 nm (L-UCNPs) were synthesized by high-temperature coprecipitation and subsequently modified with three kinds of polymers [29]. These included PEG and poly(N,N-dimethylacrylamide-co-2-aminoethylacrylamide) [P(DMA-AEA)] terminated with an alendronate anchoring group, and poly(methyl vinyl ether-co-maleic acid) (PMVEMA). To evaluate the biodistribution of the nanoparticles, 100 μL of UCNP@Ale-PEG or UCNP@Ale-(PDMA-AEA) dispersion (concentration 50 μg/mL of mouse blood) was applied retroorbitally to the mice (each nanoparticle type to 5 mice). An *in vivo* study showed that both types of nanoparticles were eliminated from the body via the liver. While L-UCNPs@Ale-PEG particles were almost completely eliminated from the liver 96 h after intravenous application, L-UCNPs@Ale-(PDMA-AEA) particles remained in the liver in a significantly higher amount. The polymeric coating can influence the retention of nanoparticles in tissues to some extent. This can be advantageously used in various applications using cell labeling in tissues and organs.

To investigate the distribution and translocation of CitNaYb0.98-xEr0.02F_4:5%Fe^{2+} UCNPs in the main organs of mice, two nude mice were intravenously injected with UCNPs (2 mg/mL, 200 mL) and, after 1 or 24 h, dissected, and their main organs (heart, lung, liver, spleen, and kidney) were examined using fluorescence molecular tomography (FMT) imaging system [61]. At both 1 and 24 h post-injection, obvious fluorescence in lung, liver, and spleen is observed. However, the fluorescence intensity in the different organs changes dramatically with time. In a short period of time (1 h), the fluorescence distribution is relatively uniform, and the fluorescence intensity is high. After 24 h, the fluorescence intensity of lung, liver, and spleen decreases significantly, especially in the lung and spleen. It is worth noting that the heart also shows a faint fluorescence. These results suggest that UCNPs may have been partially metabolized by the mice and that a small amount of UCNPs is transferred to the heart. Therefore, Cit-$NaYbF_4$:2%Er^{3+}/5%Fe^{2+} may provide visual diagnostic and therapeutic means for lung, liver, and spleen diseases.

To assess the *in vivo* biotoxicity, UCNPs-CuMnO was used in the experimental group at a concentration of 100 μL and 5 mg/mL, while the control group received the same volume of saline solution [62]. The H&E staining analysis of five main organs (heart, liver, spleen, lung and kidney) showed that there is no distinct abnormality observed 7 days after injection. These results fully demonstrate the good biocompatibility of UCNPs-CuMnO nanoprobe.

Additional decoration of the surface of nanoparticles with photodynamically active dyes has practically no effect on their toxicity.

In addition to detectability, the assessment of the new nanoparticles should also include their biocompatibility. Nanoparticles consisting of the miR-122 aptamer (Apt), UCNPs, and Prussian blue nanoparticles (PBNP) (UCNP-Apt-PBNP) were studied in recent paper [63]. To assess the safety and potential toxicity of these nanoparticles *in vivo*, a dose of 20 mg/kg UCNP-Apt-PBNP was selected, based on the amount of UCNP. This dose was the highest used in previous studies by the authors, and it was injected into mice for 14 days. The nanoparticles did not cause nephrotoxic or hepatotoxic effects, indicating their biocompatibility and potential use for imaging the liver using miR-122 targeting.

PEG-coated monodisperse UCNPs with a conjugated Flamma® fluorescent dye particles (UCNP@Ale-PEG-Flamma® particle) studied in the work [64]. Each group of mice was injected either intraperitoneally or intravenously (tail vein) with 100 ml of UCNP@Ale-PEG-Flamma® particle (0.15 mg) dispersion. After another 24 h, mice were euthanized and tumors and selected tissues (liver, kidney and muscle) were dissected. Intravenously administered UCNP@Ale-PEG-Flamma® particles accumulated strongly in the liver compared to intra peritoneal injection. The lower hepatic accumulation may be

explained by the reduced clearance rate by the mononuclear phagocytic system. In contrast, significantly increased nanoparticle accumulation in orthotopic tumors was observed in animals administered by the intraperitoneal route. The measured mean fluorescence intensity (MFI) 24 h after injection was more than 6-fold higher than that of intravenous administration. In addition, a slightly increased fluorescence signal from the kidneys of mice was observed after intravenous administration. Although insignificant, this increase may be explained by direct exposure of intravenously administered UCNPs to renal excretion mechanisms, whereas intraperitoneal administration leads to lower (and delayed) blood levels. Moreover, no differences in particle accumulation were found in skeletal muscle, which was chosen as a negative control to the remaining three tissues where accumulation was anticipated. However, this was an expected finding as there is no reason for particle accumulation in skeletal muscle. The observed differences in nanoparticle's distribution between intravenous and intraperitoneal administration may be attributed to distinct physiological barriers and clearance mechanisms involved. Intravenous administration exposes nanoparticles to immediate systemic circulation, leading to rapid clearance by organs such as the liver and kidneys. In contrast, intraperitoneal administration offers a localized delivery route that potentially bypasses some of the mechanisms of systemic clearance and allows for more targeted accumulation in peritoneal tumors. These differences in biodistribution underscore the importance of the administration route in achieving optimal therapeutic outcomes with nanoparticle-based drug delivery systems.

In the study, $Ca_{0.2}Zn_{0.9}Mg_{0.9}$ Si_2O_6 particles doped with rare earth cations (Eu^{3+}, Dy^{3+}, Mn^{3+}) and coated with PEG at a concentration of 1 mg/mL were excited with UV light (254 nm) for 5 min [65]. Subsequently, 100 mL of a colloidal solution was introduced (1 mg of stably luminescent nanoparticles was resuspended in 1 mL of sterile 150 mM NaCl). It was found that the distribution of particles in tissues highly depends on the surface coating and the core size of the particle. Smaller particles (up to 80 nm) and star shaped particles remain in circulation for a longer time, whereas PEG coatings with a molecular weight of 5 to 20 kDa have only a minor effect on the biodistribution of silica coated nanoparticles *in vivo*.

A simple fluorescence resonance energy transfer (FRET) sensing platform (termed as USP), comprised of UCNPs as the energy donor and Cy5 as the energy acceptor, has been synthesized for cathepsin B (CTSB) activity detection in vitro and *in vivo* [66]. For *in vivo* toxicity analysis, 0.2 mL stroke-physiological saline solution (0.9 wt% NaCl solution) with or without USP (10 $mg \cdot kg^{-1}$) were injected intravenously into the Kunming mice as experimental group and control group, respectively. Healthy mice were injected intravenously with USP and dissected at the 30th day post-injection. The results of body weight, histological analysis, and blood routine examination show that there is no significant difference between USP-treated mouse group and control group, demonstrating the low long-term toxicity of USP.

In study, it was developed and characterized Arg-Gly-Asp (RGD)-decorated poly-lactic-acid-co-glycolic acid (PLGA) nanoparticles for simultaneous sustained and precise co-delivery of loaded cisplatin (CDDP) (therapeutic agent) and UCNP (imaging agent) for lung cancer therapy [67]. Wistar rats were categorized ($n = 4$) in different groups and treated with CDDP loaded PLGA nanoparticles (CPF), CDDP and UCNP loaded PLGA nanoparticles (CPFT), RGD decorated CDDP and UCNP loaded PLGA nanoparticles (CPFT- RGD nanoparticles) formulations, Ciszest-50 injecion (positive control) and normal saline solution (negative control), separately. The formulations at dose of CDDP (5 mg/kg) and normal saline were administered into rats via the tail vein with an administration rate 0.4 mL/min. After 15 days and 30 days of i.v. administration of CPF, CPFT, CPFT- RGD nanoparticles and Ciszest-50 injection to rats, the morphological characteristics of collected lung tissues were assessed by standard H&E staining. In the study, the alveoli and interstitium were observed normal in the control group treated with normal saline. No pathologic lesions (i.e., inflammation, alveolar dam age, vascular and alveolar congestion) were observed in alveoli or bronchi of lung tissue. In the group treated with CPF, CPFT, CPFT-RGD nanoparticles, there was alveolar septal disruption (probably artificial) and fibrin thrombus in a few small vessels were found, with no significant alveolar hemorrhage or inflammation and bronchi are unremarkable as compared to control group. In Ciszest-50 treated group, lung parenchyma showed mild to chronic bronchial inflammation, as well as disruption of alveolar septa, small fibrin thrombi and hemorrhage. In all treated groups, no severe pathologic lesions (i.e., alveoli, bronchiole (lower right), capillaries and interstitium) were observed in the lung tissue as compared to Ciszest-50 treated groups. This result clearly indicates that CDDP loaded PLGA nanoparticles improved the biocompatibility of CDDP with lung tissue.

In tumor cells (for example, in acute lymphoblastic leukemia), asparagine is an essential amino acid; without it, the synthesis of proteins and nucleic acids is disrupted, leading to cell death.

The authors functionalized $NaYF_4$ UCNPs with isocyanate groups and then immobilized the enzyme pegylated L asparaginase (L-ASNase) (PEG-L-ASNase) via covalent bonding [68]. As noted above, pegylation of the surface reduces the toxicity of nanoparticles.

The nanoparticles injected into mice were irradiated with a 150 mW laser at 808 nm for 30 min at a distance of 1 cm. The histological pattern of heart and liver tissues did not change compared to the control. In kidney tissues, a slight increase in the density of degenerated cells in the renal medulla was observed in

the case of non pegylated UCNPs and after laser irradiation. In the same groups of mice, an increased density of degenerated cells was found in spleen tissues, and giant cells with nuclei were detected.

However, in the literature, similar tissues were histopathologically examined in *in vivo* studies with UCNPs containing various functional groups, and it was indicated that the toxic damage was minor [42, 69, 70].

At 48 h post-UCNP administration, high concentrations of Er^{3+} were observed in the spleen, while Er^{3+} levels remained quite low in the liver, heart, and kidneys.

Zhao and others reported that nanoparticles (NPs), which are considered foreign objects, primarily accumulate in the liver and spleen [71].

Since the biodistribution of nanomaterials is dictated by their surface chemistry – which affects the extent and specificity of protein binding – modification with PEG-L-ASNase could facilitate the elimination of UCNPs from the body and prevent long term accumulation after intravenous administration [70]. Consequently, such particles can be safely used for *in vivo* administration.

When a suspension of $NaGdF_4$:Tm^{3+}, Er^{3+}, Yb^{3+} particles coated with oleic acid oxidized to azelaic acid was administered (volume: 150 μL; concentration: 1 mg/mL), their high relaxivity of 5,60 $s^{-1}mM^{-1}$ was demonstrated [72].

These nanoparticles were successfully used as contrast agents for *in vivo* MRI [73].

The dependence of toxicity on such parameters as particle type, particle coating type, dose, concentration and method of particle administration, summarizing the reviewed articles, is presented in Table 1.

Table 1 Dependence of toxicity on such parameters as particle type, particle coating type, dose, concentration and method of particle administration.

UCNP type	Coating	Charge	Type of animal	Dose (mg/kg)	Concentration (mg/ml)	Route of administration	Main results (toxicity etc.)	Ref.
$NaYF_4$:Yb^{3+}/ Er^{3+}	PEG	Not specified (neutral)	BALB/c mice	2.0 mg [Y]/kg (high), 0.2 mg [Y]/kg (low)	Not specified	Intravenous (tail vein)	No histopathological damage in heart, liver, spleen, lungs, kidneys at 24 and 72 h; no inflammation; complete elimination in 72 h via feces then urine	[50]
$NaYF_4$:Yb^{3+}/ Tm^{3+}	SiO_2	Not specified	Rats	10	Not specified	Intravenous	No adverse health effects or behavioral changes for 7 days	[33,34]
$NaYF_4$:Yb/Er	SiO_2	Not specified	Mice	100	Not specified	Oral or intravenous	No significant toxicity; oral → accumulation in bones, stomach, intestines; i.v. → liver and spleen	[35]
$NaYF_4$:Yb^{3+}, Er^{3+}	PEI	Positive	Rats	10	0.0015, 0.01, 0.015, 0.025	Intravenous	No toxic effects on cells or mice	[36]
$NaYF_4$:Yb,Er	PEI	Positive	Mice	10	Not specified	Intravenous, intraperitoneal, intragastric	Intraperitoneal → spleen accumulation for 30 days; intragastric → ileum and cecum; i.v. → excretion within 30 days	[37,38]

Table 1 (Cont.)

$NaYF_4$:20% Yb^{3+},1%Tm^{3+}	PAA	Negative	Mice	15	Not specified	Intravenous	No toxic effects; minor hyperplasia in splenic white pulp	[40]
$NaYF_4$:Yb^{3+}/ Tm^{3+}	PEG or PAA	Neutral (PEG) / Negative (PAA)	Mice	20	2	Intravenous	No noticeable toxic side effects up to 90 days; no histological damage	[42]
β-$NaYF_4$: 20%Yb^{3+},2% Tm^{3+}	Octylamine-PAA or DSPE-PEG	Negative (PAA) / Neutral (PEG)	Mice	20	2	Intravenous (vena cava)	No histological damage or organ impairment; biochemical/ hematological analyses normal	[42]
NaYF:Yb,Er (25 nm and 120 nm)	Ale-PEG or Ale-(PDMA-AEA)	Not specified	Mice	~5 (based on 50 μg/ml blood, 100 μl)	0.05 (in blood)	Retroorbital	Both eliminated via liver; L-UCNPs@Ale-PEG almost fully cleared at 96 h; L-UCNPs@Ale-(PDMA-AEA) remained longer	[29]
Cit-$NaYbF_4$:2% Er^{3+}/5%Fe^{2+}	Citrate	Negative	Nude mice	~40 (2 mg/ml × 0.2 ml for ~20 g mouse)	2	Intravenous	Fluorescence in lung, liver, spleen at 1 and 24 h; decreased by 24 h; faint signal in heart	[61]
UCNPs-CuMnO	Not specified (likely PEG or similar)	Not specified	Mice	~25 (5 mg/ml × 0.1 ml for ~20 g mouse)	5	Not specified (likely intravenous)	No distinct abnormality in H&E staining of heart, liver, spleen, lung, kidney at 7 days	[62]
UCNP-Apt-PBNP (miR-122 aptamer)	Not specified (Apt-PBNP)	Not specified	Mice	20	Not specified	Not specified	No nephrotoxic or hepatotoxic effects after 14 days	[63]
UCNP@Ale-PEG-Flamma®	PEG + Flamma® dye	Not specified	Mice	~7.5 (0.15 mg per mouse, ~20 g)	Not specified	Intraperitoneal vs. intravenous	i.v. → high liver accumulation; i.p. → lower liver accumulation, 6× higher tumor accumulation	[64]

Table 1 (Cont.)

$Ca_{0.2}Zn_{0.9}Mg_{0.9}Si_2O_6:Eu^{3+},Dy^{3+},Mn^{3+}$	PEG	Not specified	Mice	~5 (1 mg/ml × 0.1 ml for ~20 g mouse)	1	Not specified (likely i.v. or i.p.)	Distribution depends on size and shape; smaller (<80 nm) and star-shaped remain longer in circulation	[65]
UCNP-Cy5 (USP, FRET sensor)	Not specified	Not specified	Kunming mice	10	Not specified	Intravenous	No significant difference in body weight, histology, blood routine at 30 days; low long-term toxicity	[66]
CDDP + UCNP in PLGA (CPFT-RGD)	PLGA + RGD	Not specified	Wistar rats	5 (as CDDP)	Not specified	Intravenous (0.4 ml/min)	No severe pathologic lesions in lung tissue; improved biocompatibility compared to free cisplatin	[67]
$NaYF_4$ with PEG-L-ASNase	PEG-L-asparaginase	Not specified	Mice	Not specified	Not specified	Not specified	No heart/liver changes; slight renal medulla degeneration in non-PEG group after laser; spleen giant cells in non-PEG + laser	[68]
$NaGdF_4:Tm^{3+}Er^{3+},Yb^{3+}$	Azelaic acid (from oleic acid oxidation)	Negative	Not specified (MRI study)	~0.15 (150 µl × 1 mg/ml for ~1 kg assumed, but not specified)	1	Not specified	Used as MRI contrast agent; relaxivity 5.60 $s^{-1}mM^{-1}$; no toxicity reported explicitly	[72,73]

Note: "Not specified" indicates the original article did not report the parameter.

Doses in mg/kg were calculated where possible based on typical mouse body weight (20 g) and injection volume; some values are approximate.

Charge assignments are based on known properties of coatings: PEI (+), PAA (−), PEG (neutral), PVP (neutral).

3 Conclusion

This review (Part I) has synthesized current knowledge on the *in vivo* dark toxicity of upconversion nanoparticles (UCNPs), with a focus on the physicochemical and physiological factors that determine their safety profile for biomedical applications. Based on comprehensive histological, biochemical, and hematological analyses reported in the literature, the following conclusions can be drawn.

UCNPs generally demonstrate low dark toxicity under tested conditions, provided that their surface is appropriately stabilized. The primary mechanism of dark toxicity is the dissolution of nanoparticles leading to the release of rare-earth ions (e.g., Y^{3+}, Yb^{3+}, Er^{3+}) and fluoride ions, which can accumulate in organs such as the liver, spleen, and bones. However, at recommended doses, no significant organ damage or adverse behavioral changes have been observed.

The toxicity of UCNPs is strongly modulated by their surface coating. Silica (SiO_2) coatings reduce solubility and fluoride ion release, showing low cytotoxicity at doses up to 100 mg/kg in mice. Polyethylene glycol (PEG) coatings provide excellent biocompatibility, reduce protein adsorption, and prolong circulation time without evident toxicity at 20 mg/kg. Polyacrylic acid (PAA) coatings (negatively charged) exhibit the lowest cytotoxicity among tested polymers, with no significant toxicity observed over 115 days at 15 mg/kg. Polyethyleneimine (PEI) coatings (positively charged) enhance cellular internalization but may induce membrane disruption and cytotoxicity at high molecular weights and concentrations; however, lower concentrations (10 mg/kg) have shown no toxic effects. Neutral coatings (PVP) demonstrate intermediate toxicity and penetration efficiency.

Positively charged UCNPs (e.g., PEI-coated) exhibit higher cellular uptake due to electrostatic attraction to negatively charged cell membranes, but also higher cytotoxicity. Negatively charged (PAA) and neutral (PVP) particles are less toxic, albeit with reduced penetration efficiency.

Based on a critical review of available evidence, the maximum permissible concentration of UCNPs is estimated at 2 mg/mL. The following dose regimens are recommended as safe for *in vivo* applications: for mice are 10 mg/kg for short-term exposure (12 h) and 50 mg/kg for long-term exposure (120 days); for rats is 5 mg/kg for both short- and long-term exposure. This choice is based on minimal or no changes in the internal organs based on the results of histology.

UCNPs primarily accumulate in the liver and spleen following intravenous administration, with partial clearance via fecal and urinary routes. Complete elimination has been reported within 72 h for PEG-coated particles and within 30 days for PEI-coated particles. Intraperitoneal administration may reduce hepatic accumulation compared to intravenous injection. Intravenous administration of PEI-coated UCNPs led to gradual excretion from the body within 30 days and decreasing accumulation in the spleen. In contrast, intraperitoneal administration resulted in significant particle accumulation in the spleen for up to 30 days. Following intragastric administration, UCNPs were primarily detected in the ileum and cecum, with relatively low presence in other organs. Intravenous injection of PEGylated or PAA-coated nanoparticles caused no evident histological damage or organ impairment, with particles accumulating mainly in the liver and spleen.

Across numerous studies, H&E staining of major organs (heart, liver, spleen, lungs, kidneys) from UCNP-treated animals showed no significant inflammatory responses, necrosis, or morphological abnormalities compared to controls, except for minor, reversible changes such as transient hyperplasia in the splenic white pulp.

Smaller UCNPs (below 100 nm) are preferred for tissue penetration but may pose higher reactivity risks. Particle size and shape (e.g., spherical vs. hexagonal) influence biodistribution and retention time, with smaller particles remaining in circulation longer.

Decoration of UCNPs with targeting ligands (e.g., RGD peptides, aptamers) or photodynamically active dyes has been shown to have minimal additional toxic effects, supporting their use in multimodal theranostic platforms.

In summary, UCNPs represent a promising class of luminescent nanomaterials for *in vivo* imaging and therapy, with an acceptable safety profile at established concentrations and doses. However, the heterogeneity of experimental conditions across studies – particularly variations in coating materials, administration routes, and exposure durations – underscores the need for standardized toxicity assessment protocols. Part II of this review will address the phototoxicity of UCNPs, while Part III will examine the toxicity of multimodal upconversion particles.

Disclosures

All authors declare that there is no conflict of interests in this paper.

Acknowledgements

The study was supported by a grant Russian Science Foundation No. 25-22-00144, https://rscf.ru/project/25-22-00144/.

References

1. S. Hong, S. Rhee, and K. O. Jung, "*In vivo* molecular and single cell imaging," BMB Reports 55(6), 267–274 (2022).
2. M. Woźniak, A. Płoska, A. Siekierzycka, L. W. Dobrucki, L. Kalinowski, and I. T. Dobrucki, "Molecular Imaging and Nanotechnology—Emerging Tools in Diagnostics and Therapy," International Journal of Molecular Sciences 23(5), 2658 (2022).
3. J. C. L. Chow, "Nanomaterial-Based Molecular Imaging in Cancer: Advances in Simulation and AI Integration," Biomolecules 15(3), 444 (2025).
4. N. W. Nkune, K. Moloudi, B. P. George, and H. Abrahamse, "An update on recent advances in fluorescent materials for fluorescence molecular imaging: a review," RSC Advances 15(28), 22267–22284 (2025).
5. Y. Tang, Y. Li, C. He, Z. Wang, W. Huang, Q. Fan, and B. Liu, "NIR-II-excited off-on-off fluorescent nanoprobes for sensitive molecular imaging *in vivo*," Nature Communications 16(1), 278 (2025).

6. K. Lu, R. Zhang, H. Wang, C. Li, Z. Yang, K. Xu, X. Cao, N. Wang, W. Cai, J. Zeng, and M. Gao, "PEGylated Ultrasmall Iron Oxide Nanoparticles as MRI Contrast Agents for Vascular Imaging and Real-Time Monitoring," ACS Nano 19(3), 3519–3530 (2025).
7. W. Zhang, X. Chen, D. Ding, G. Zhang, Z. Zhu, X. Yang, M. Li, L. Liang, X. Shi, T. Wang, and R. Gao, "Real-time *in vivo* imaging reveals specific nanoparticle target binding in a syngeneic glioma mouse model," Nanoscale 14(15), 5678–5688 (2022).
8. Y. Yang, Y. Chen, P. Pei, Y. Fan, S. Wang, H. Zhang, D. Zhao, B.-Z. Qian, and F. Zhang, "Fluorescence-amplified nanocrystals in the second near-infrared window for *in vivo* real-time dynamic multiplexed imaging," Nature Nanotechnology 18(10), 1195–1204 (2023).
9. S. Liu, W. Dong, H. Gao, Z. Song, and Z. Cheng, "Near-Infrared-II Fluorescent Probes for Analytical Applications: From In Vitro Detection to *In Vivo* Imaging Monitoring," Accounts of Chemical Research 58(4), 543–554 (2025).
10. R. Luo, C. Zhang, Z. Zhang, P. Ren, Z. Xu, and Y. Liu, "NIR-II upconversion nanomaterials for biomedical applications," Nanoscale 17(6), 2985–3002 (2025).
11. V. C. Thipe, A. R. Karikachery, P. Çakılkaya, U. Farooq, H. H. Genedy, N. Kaeokhamloed, D.-H. Phan, R. Rezwan, G. Tezcan, E. Roger, and K. V. Katti, "Green nanotechnology—An innovative pathway towards biocompatible and medically relevant gold nanoparticles," Journal of Drug Delivery Science and Technology 70, 103256 (2022).
12. A. Pavlou, A. Katsouras, M. Markou, A. Nega, S. Bellou, P. Koralli, A. Schiza, N. Chalmpes, V. G. Gregoriou, A. Dimitrakopoulou-Strauss, T. Fotsis, A. Avgeropoulos, M. G. Siskos, C. Murphy, and C. L. Chochos, "Rational Design of New Biocompatible Near-Infrared Conjugated Polymer Nanoparticles for Biomedical Applications," Macromolecules 59(3), 1429–1442 (2026).
13. C.-Y. Zhong, L. Xiao, J. Zhou, Z. Chen, Y. Chen, Z.-Q. Liu, and J. Z. Zhang, "Two-photon photoluminescence and bio-imaging application of monodispersed perovskite-in-silica nanocrystals with high biocompatibility," Chemical Engineering Journal 431, 134110 (2022).
14. A. Schroter and T. Hirsch, "Control of Luminescence and Interfacial Properties as Perspective for Upconversion Nanoparticles," Small 20(14), 2306042 (2024).
15. E. M. Mettenbrink, W. Yang, and S. Wilhelm, "Bioimaging with Upconversion Nanoparticles," Advanced Photonics Research 3(12), 2200098 (2022).
16. Y. Yang, Y. Xie, and F. Zhang, "Second near-infrared window fluorescence nanoprobes for deep-tissue *in vivo* multiplexed bioimaging," Advanced Drug Delivery Reviews 193, 114697 (2023).
17. Z. Su, Y. Zhao, Y. Lian, Y. Li, B. Lou, C.-G. Ma, B. Xu, J. Dong, and G. Bai, "Multifunctional lanthanide-doped nanoparticles enabled fiber probe with decoupled modules for tumor therapy and real-time temperature sensing," Science China Materials 69(1), 139–148 (2026).
18. S. Gulati, R. Yadav, V. Kumari, S. Nair, C. Gupta, and M. Aishwari, "Nanosensors in healthcare: transforming real-time monitoring and disease management with cutting-edge nanotechnology," RSC Pharmaceutics 2(5), 1003–1018 (2025).
19. Y. Ma, M. Song, L. Li, X. Lao, M. Wong, and J. Hao, "Advances in upconversion luminescence nanomaterial-based biosensor for virus diagnosis," Exploration 2(6), 20210216 (2022).
20. J. Zhao, Z. Di, and L. Li, "Spatiotemporally Selective Molecular Imaging via Upconversion Luminescence-Controlled, DNA-Based Biosensor Technology," Angewandte Chemie International Edition 61(32), e202204277 (2022).
21. I. Yu. Yanina, E. K. Volkova, E. A. Sagaidachnaya, Ju. G. Konyukhova, V. I.Kochubey, and V. V. Tuchin, "Comparison of temperature sensing of the luminescent upconversion and ZnCdS nanoparticles," Proceedings of SPIE 10506, 1050616 (2018).
22. A. Molkenova, H. E. Choi, J. M. Park, J.-H. Lee, and K. S. Kim, "Plasmon Modulated Upconversion Biosensors," Biosensors 13(3), 306 (2023).
23. G. De Freitas Silva, G. De Lima Fernandes, J. H. Faleiro, T. K. De Lima Rezende, H. P. Barbosa, and J. L. Ferrari, "Biosensing Based on Upconversion Nanoparticles," in Upconversion Nanoparticles (UCNPs) for Functional Applications, V. Kumar, I. Ayoub, H. C. Swart, and R. Sehgal (Eds.), Springer Nature Singapore, 24, 369–403 (2023).
24. Y. Li, C. Chen, F. Liu, and J. Liu, "Engineered lanthanide-doped upconversion nanoparticles for biosensing and bioimaging application," Microchimica Acta 189(3), 109 (2022).
25. X. Wang, C. Jiang, Z. Wang, B. E. Cohen, E. M. Chan, and G. Chen, "Triplet-Induced Singlet Oxygen Photobleaches Near-Infrared Dye-Sensitized Upconversion Nanosystems," Nano Letters 23(15), 7001–7007 (2023).
26. N. Singh, R. Sen Gupta, and S. Bose, "A comprehensive review on singlet oxygen generation in nanomaterials and conjugated polymers for photodynamic therapy in the treatment of cancer," Nanoscale 16(7), 3243–3268 (2024).
27. M. Przygoda, D. Bartusik-Aebisher, K. Dynarowicz, G. Cieślar, A. Kawczyk-Krupka, and D. Aebisher, "Cellular Mechanisms of Singlet Oxygen in Photodynamic Therapy," International Journal of Molecular Sciences 24(23), 16890 (2023).

28. I. A. Khan, T. Yu, M. Yang, J. Liu, and Z. Chen, "A Systematic Review of Toxicity, Biodistribution, and Biosafety in Upconversion Nanomaterials: Critical Insights into Toxicity Mitigation Strategies and Future Directions for Safe Applications," BME Frontiers 6, 0120 (2025).
29. L. Machová Urdzíková, D. Mareková, T. Vasylyshyn, P. Matouš, V. Patsula, V. Oleksa, O. Shapoval, M. Vosmanská, D. Liebl, A. Benda, V. Herynek, D. Horák, and P. Jendelová, "Toxicity of Large and Small Surface-Engineered Upconverting Nanoparticles for *In Vitro* and *In Vivo* Bioapplications," International Journal of Molecular Sciences 25(10), 5294 (2024).
30. S. Märkl, F. Przybilla, R. Rachel, T. Hirsch, M. Keller, R. Witzgall, Y. Mély, and J. Wegener, "Impact of surface chemistry of upconversion nanoparticles on time-dependent cytotoxicity in non-cancerous epithelial cells," Scientific Reports 14(1), 30610 (2024).
31. S. Hofer, N. Hofstätter, B. Punz, I. Hasenkopf, L. Johnson, and M. Himly, "Immunotoxicity of nanomaterials in health and disease: Current challenges and emerging approaches for identifying immune modifiers in susceptible populations," Wiley Interdisciplinary Reviews: Nanomedicine and Nanobiotechnology 14(6), e1804 (2022).
32. M. M. Rahman, J. Uddin, A. M. Asiri, and M. R. Rahman (Eds.), Toxicity of Nanoparticles-Recent Advances and New Perspectives: Recent Advances and New Perspectives, IntechOpen, London, United Kingdom (2024). eBook ISBN: 978-1-83768-605-6.
33. R. Abdul Jalil, Y. Zhang, "Biocompatibility of silica coated $NaYF_4$ upconversion fluorescent nanocrystals," Biomaterials 29(30), 4122–4128 (2008).
34. F. Wang, D. Banerjee, Y. Liu, X. Chen, and X. Liu, "Upconversion nanoparticles in biological labeling, imaging, and therapy," Analyst 135(8), 1839 (2010).
35. M. Zhou, X. Ge, D.-M. Ke, H. Tang, J.-Z. Zhang, M. Calvaresi, B. Gao, L. Sun, Q. Su, and H. Wang, "The Bioavailability, Biodistribution, and Toxic Effects of Silica-Coated Upconversion Nanoparticles *in vivo*," Frontiers in Chemistry 7, 218 (2019).
36. D. K. Chatterjee, A. J. Rufaihah, and Y. Zhang, "Upconversion fluorescence imaging of cells and small animals using lanthanide doped nanocrystals," Biomaterials 29(7), 937–943 (2008).
37. J. Yu, W. Yin, T. Peng, Y. Chang, Y. Zu, J. Li, X. He, X. Ma, Z. Gu, and Y. Zhao, "Biodistribution, excretion, and toxicity of polyethyleneimine modified $NaYF_4$:Yb,Er upconversion nanoparticles in mice via different administration routes," Nanoscale 9(13), 4497–4507 (2017).
38. N. Long, W.-T. Wong (Eds.), The Chemistry of Molecular Imaging, John Wiley & Sons (2014). ISBN: 978-1-118-09327-6
39. J. F. Jin, Y. J. Gu, C. W. Y. Man, J. P. Cheng, Z. H. Xu, Y. Zhang, H. S. Wang, V. H. Y. Lee, S. H. Cheng, and W. T. Wong, "Polymer-coated $NaYF_4$:Yb^{3+}, Er^{3+} upconversion nanoparticles for charge-dependent cellular imaging," ACS Nano 5(10), 7838–7847 (2011).
40. L. Xiong, T. Yang, Y. Yang, C. Xu, and F. Li, "Long-term *in vivo* biodistribution imaging and toxicity of polyacrylic acid-coated upconversion nanophosphors," Biomaterials 31(27), 7078–7085 (2010).
41. X. Sun, J. Shi, X. Fu, Y. Yang, and H. Zhang, "Long-term *in vivo* biodistribution and toxicity study of functionalized near-infrared persistent luminescence nanoparticles," Scientific Reports 8(1), 10595 (2018).
42. L. Cheng, K. Yang, M. Shao, X. Lu, and Z. Liu, "*In Vivo* Pharmacokinetics, Long-Term Biodistribution and Toxicology Study of Functionalized Upconversion Nanoparticles in Mice," Nanomedicine 6(8), 1327–1340 (2011).
43. J. Li, X. Chang, X. Chen, Z. Gu, F. Zhao, Z. Chai, and Y. Zhao, "Toxicity of inorganic nanomaterials in biomedical imaging," Biotechnology Advances 32(4), 727–743 (2014).
44. M. Z. Ahmad, B. A. Abdel-Wahab, A. Alam, S. Zafar, J. Ahmad, F. J. Ahmad, P. Midoux, C. Pichon, and S. Akhter, "Toxicity of Inorganic Nanoparticles Used in Targeted Drug Delivery and Other Biomedical Application: An Updated Account on Concern of Biomedical Nanotoxicology," Journal of Nanoscience and Nanotechnology 16(8), 7873–7897 (2016).
45. A. Gnach, T. Lipinski, A. Bednarkiewicz, J. Rybka, and J. A. Capobianco, "Upconverting nanoparticles: assessing the toxicity," Chemical Society Reviews 44(6), 1561–1584 (2015).
46. C. Dai, S. Chen, C. Wang, L. Zhang, K. Ge, and J. Zhang, "Ytterbium ion promotes apoptosis of primary mouse bone marrow stromal cells?," Journal of Rare Earths 33(4), 445–452 (2015).
47. K. A. Gschneidner, J.-C. G. Bünzli, and V. K. Pecharsky, "Preface," in Handbook on the Physics and Chemistry of Rare Earths, K. A. Gschneidner, J.-C. G. Bünzli, and V. K. Pecharsky (Eds.), 37, Elsevier, v–x (2007).
48. B. Tian, Q. Wang, Q. Su, W. Feng, and F. Li, "*In vivo* biodistribution and toxicity assessment of triplet-triplet annihilation-based upconversion nanocapsules," Biomaterials 112, 10–19 (2017).
49. R. Yang, L. Cai, A. Zheng, and J. Guan, "Inhalation of upconversion nanoparticles does transient damage to the mouse liver and lung," Chinese Journal of Tissue Engineering Research 20 (52), 7865–7871 (2016).
50. S. Wang, H. Liang, Z. Yang, Z. Wang, B. Yang, and C. Lu, "Direct large-scale synthesis of water-soluble and biocompatible upconversion nanoparticles for *in vivo* imaging," RSC Advances 14(25), 17350–17354 (2024).
51. B. Fubini, A. Hubbard, "Reactive oxygen species (ROS) and reactive nitrogen species (RNS) generation by silica in inflammation and fibrosis," Free Radical Biology and Medicine 34(12), 1507–1516 (2003).
52. D. B. Warheit, "Nanoparticles: health impacts?," Materials Today 7(2), 32–35 (2004).

53. V. Bastos, P. Oskoei, E. Andresen, M. I. Saleh, B. Rühle, U. Resch-Genger, and H. Oliveira, "Stability, dissolution, and cytotoxicity of NaYF4-upconversion nanoparticles with different coatings," Scientific Reports 12(1), 3770 (2022).
54. F. Chen, W. Bu, W. Cai, and J. Shi, "Functionalized Upconversion Nanoparticles: Versatile Nanoplatforms for Translational Research," Current Molecular Medicine 13(10), 1613–1632 (2013).
55. Z. Yu, Y. Xia, J. Xing, Z. Li, J. Zhen, Y. Jin, Y. Tian, C. Liu, Z. Jiang, J. Li, and A. Wu, "Y1 -receptor–ligand-functionalized ultrasmall upconversion nanoparticles for tumor-targeted trimodality imaging and photodynamic therapy with low toxicity," Nanoscale 10(36), 17038–17052 (2018).
56. L. Sun, Z. Wei, H. Chen, J. Liu, J. Guo, M. Cao, T. Wen, and L. Shi, "Folic acid-functionalized up-conversion nanoparticles: toxicity studies *in vivo* and *in vitro* and targeted imaging applications," Nanoscale 6(15), 8878–8883 (2014).
57. J. Zhang, F. Liu, T. Li, X. He, and Z. Wang, "Surface charge effect on the cellular interaction and cytotoxicity of $NaYF_4:Yb^{3+}$, Er^{3+}@SiO2 nanoparticles," RSC Advances 5(10), 7773–7780 (2015).
58. A. E. Guller, A. N. Generalova, E. V. Petersen, A. V. Nechaev, I. A. Trusova, N. N. Landyshev, A. Nadort, E. A. Grebenik, S. M. Deyev, A. B. Shekhter, and A. V. Zvyagin, "Cytotoxicity and non-specific cellular uptake of bare and surface-modified upconversion nanoparticles in human skin cells," Nano Research 8(5), 1546–1562 (2015).
59. S. Maiolino, A. Russo, V. Pagliara, C. Conte, F. Ungaro, G. Russo, and F. Quaglia, "Biodegradable nanoparticles sequentially decorated with Polyethyleneimine and Hyaluronan for the targeted delivery of docetaxel to airway cancer cells," Journal of Nanobiotechnology 13(1), 29 (2015).
60. H. Yang, Y. Li, T. Li, M. Xu, Y. Chen, C. Wu, X. Dang, and Y. Liu, "Multifunctional Core/Shell Nanoparticles Cross-linked Polyetherimide-folic Acid as Efficient Notch-1 siRNA Carrier for Targeted Killing of Breast Cancer," Scientific Reports 4(1), 7072 (2014).
61. X. Luo, Q. Chen, H. Guo, H. Zhang, X. He, and W. Zhao, "One-step hydrothermal synthesis of Cit-$NaYb_{F4}:E^{r3+}$ nanocrystals with enhanced red upconversion emission for *in vivo* fluorescence molecular tomography," Journal of Rare Earths 42(1), 36–45 (2024).
62. S. Yan, G. Xing, X. Yuan, E. Cui, K. Ji, X. Yang, J. Su, D. Mara, J. Tang, Y. Zhao, J. Hu, and J. Liu, "Upconversion nanoparticles-$CuMnO_2$ nanoassemblies for NIR-excited imaging of reactive oxygen species *in vivo*," Journal of Colloid and Interface Science 677, 666–674 (2025).
63. Q.-L. Wang, L.-C. Meng, Z. Zhao, J.-F. Du, P. Li, Y. Jiang, and H.-J. Li, "Ultrasensitive upconverting nanoprobes for in situ imaging of drug-induced liver injury using miR-122 as the biomarker," Talanta 274, 126108 (2024).
64. T. Vasylyshyn, V. Patsula, D. Větvička, O. Shapoval, J. Pankrác, M. Kabešová, J. Beneš, and D. Horák, "Intraperitoneal versus intravenous administration of Flamma®-conjugated PEG-alendronate-coated upconversion nanoparticles in a mouse pancreatic cancer model," Nanoscale Advances 7(1), 144–154 (2025).
65. T. Maldiney, C. Richard, J. Seguin, N. Wattier, M. Bessodes, and D. Scherman, "Effect of Core Diameter, Surface Coating, and PEG Chain Length on the Biodistribution of Persistent Luminescence Nanoparticles in Mice," ACS Nano 5(2), 854–862 (2011).
66. X. Li, M. Zhang, H. Zhang, Z. Wang, and H. Zhang, "Upconversion nanoparticle-based fluorescence resonance energy transfer sensing platform for the detection of cathepsin B activity *in vitro* and *in vivo*," Microchimica Acta 190(5), 181 (2023).
67. B. Yadav, M. Chauhan, S. Shekhar, A. Kumar, A. K. Mehata, A. K. Nayak, R. Dutt, V. Garg, V. Kailashiya, M. S. Muthu, Sonali, and R. P. Singh, "RGD-decorated PLGA nanoparticles improved effectiveness and safety of cisplatin for lung cancer therapy," International Journal of Pharmaceutics 633, 122587 (2023).
68. B. Ateş, A. Ulu, M. Asiltürk, S. A. A. Noma, S. D. Topel, G. Dik, O. Özhan, B. Bakar, A. Yıldız, N. Vardı, and H. Parlakpınar, "Enhancement of enzyme activity by laser-induced energy propulsion of upconverting nanoparticles under near-infrared light: A comprehensive methodology for *in vitro* and *in vivo* applications," International Journal of Biological Macromolecules 260, 129343 (2024).
69. Y. Bai, Y. Li, R. Wang, and Y. Li, "Low Toxicity, High Resolution, and Red Tissue Imaging in the Vivo of Yb/Tm/GZO@SiO_2 Core–Shell Upconversion Nanoparticles," ACS Omega 5(10), 5346–5355 (2020).
70. H. Zhao, W. Hu, H. Ma, R. Jiang, Y. Tang, Y. Ji, X. Lu, B. Hou, W. Deng, W. Huang, and Q. Fan, "Photo-Induced Charge-Variable Conjugated Polyelectrolyte Brushes Encapsulating Upconversion Nanoparticles for Promoted siRNA Release and Collaborative Photodynamic Therapy under NIR Light Irradiation," Advanced Functional Materials 27(44), 1702592 (2017).
71. Y. Zhao, D. Sultan, and Y. Liu, "Biodistribution, Excretion, and Toxicity of Nanoparticles," Chapter 2 in Theranostic Bionanomaterials, W. Cui, X. Zhao (Eds.), Elsevier, 27–53 (2019).
72. N. Ghafoor, K. Javed, U. E. Ummara, N. Anees, T. Mehar, U. Khursheed, R. Shahid, and A. Ghafoor, "Nanoparticles in diagnostic imaging: advancements and challenges," in Complementary and Alternative Medicine: Nanotechnology I, V. G. G. Rubio, A. Khan, S. Altaf, Z. Saeed, and W. Qamar (Eds.), Unique Scientific Publishers, Faisalabad, Pakistan, 276–284 (2024).

73. J. Zhou, Y. Sun, X. Du, L. Xiong, H. Hu, and F. Li, "Dual-modality *in vivo* imaging using rare-earth nanocrystals with near-infrared to near-infrared (NIR-to-NIR) upconversion luminescence and magnetic resonance properties," Biomaterials 31(12), 3287–3295 (2010).